Journal of Structural Geology, Vol. 15, No. 9/10, pp. 1169 to 1187, 1993
Printed in Great Britain

0191-8141/93 $06.00+0.00

Individual orientation measurements in quartz polycrystals: advantages and limitations for texture and petrophysical property determinations

DAVID MAINPRICE

Laboratoire de Tectonophysique, URA 1370 CNRS and Université Montpellier II, Place E. Bataillon, 34095 Montpellier Cédex 05, France

GEOFFREY E. LLOYD

Department of Earth Sciences, University of Leeds, Leeds LS2 9JT, U.K.

and

MARTIN CASEY

Geologisches Institut, ETH-Zentrum, CH-8092 Zürich, Switzerland

(*Received* 5 *August* 1992; *accepted in revised form* 8 *February* 1993)

Abstract—Individual orientation determination of quartz grains by electron channelling in principle gives the complete orientation. However, in routine analysis the noise level in electron channelling patterns (ECPs) does not permit the determination of handedness of a quartz grain in a polycrystal. In practice, all quartz grains are arbitrarily indexed as right-handed. Hence, Dauphiné twins can be identified, but not Brazil twins. This practice also means that only the centrosymmetric petrophysical properties can be determined from texture measurements. These include most geologically relevant properties (e.g. thermal conductivity, thermal expansion and elasticity). However, other properties (e.g. piezoelectricity) which are not centrosymmetric cannot be calculated from such texture measurements. Some texture-forming processes (e.g. dislocation glide) can also be considered to be centrosymmetric in quartz, whereas others (e.g. grain boundary migration) may not be.

The method of quantitative texture analysis from individual measurements is briefly recalled. As an example, 382 grains from Tongue quartzite are used to illustrate the advantages of texture analysis from ECPs. The orientation distribution function (ODF) is calculated from ECPs and X-ray pole figures of the same sample. The agreement is found to be good between the two methods, proving that ECPs can be used for quantitative analysis. The methods used in local texture analysis and the definitions of the various misorientation distribution functions (MODFs) are given. Data collected from a traverse of a quartzo-feldspathic shear zone in Lewisian gneiss (Torridon 'quartzite') are used to illustrate local texture analysis. Examples from a region of shear strain of about one are given of core and mantle subgrains and Dauphiné twins. Dispersion trails of the crystallographic axes within a single grain show an apparent rotation about the intermediate structural axis *Y*. Detailed analysis of the subgrain misorientation axes in specimen and crystallographic co-ordinates show an important scatter, implying that the subgrains resulted from local incompatibility strains rather than specimen-scale kinematics.

The method of calculation of physical properties from individual orientation measurements is given for second- and fourth-order tensors. Using the texture data from Tongue quartzite we have calculated thermal conductivity, thermal expansion and seismic velocities. All these properties are extremely anisotropic in quartz. However, it is emphasized that the presence of a second phase on grain boundaries (e.g. water, graphite) may completely alter a physical property (e.g. electric) and render the values calculated from texture measurements inappropriate.

INTRODUCTION

IN QUANTITATIVE texture analysis (e.g. Bunge 1982) the bulk diffraction techniques of X-ray and neutron texture goniometry have dominated routine analysis. These classic techniques are particularly well adapted to the study of pure fine-grained (<200 μm) homogeneous specimens of high crystal and sample symmetries (e.g. axial) such as produced by metallurgical or experimental rock deformation studies (Wenk 1985). Natural deformation more frequently produces heterogeneous polyphased samples of variable grain size and low specimen symmetry (e.g. triclinic). Some aspects of the texture of coarse-grained polyphased specimens can be studied by neutron diffraction texture goniometry combined with a position sensitive detector, even those containing triclinic crystal symmetry phases (e.g. plagioclase, Wenk *et al.* 1986). However, access to neutron diffraction facilities is limited and the data processing involved in the deconvolution of the pole figures from the continuous Bragg angle (2θ) scan is extremely time consuming and hence not suited to routine analysis.

The traditional technique used by Earth Scientists for texture (or crystallographic fabric as it is more often called) analysis is the optical microscope equipped with a universal (U) stage. This is an individual orientation technique which allows the study of heterogeneous, optically transparent polyphase specimens. The small-

est grain size one can study is typically 30 μm, although this varies slightly from mineral to mineral. The method relies on the identification of the orientation of the optical indicatrix, and in many cases additional crystallographic features (e.g. twins, cleavages), for the complete orientation determination. Textures comprising complete individual orientation determinations have been derived for most of the principal rock-forming minerals (e.g. calcite, dolomite, olivine, orthopyroxene, clinopyroxene and plagioclase). The major exception is quartz where only the *c*-axis fabric can be determined by optical methods and hence quantitative texture analysis has almost exclusively been undertaken using X-ray or neutron diffraction with the limitations that this imposes.

The U-stage has proved a valuable tool, albeit time consuming for fabric studies. The routine absolute orientation determination is about ±5°, with relative orientation determinations between neighbouring grain or subgrains being about ±3°. In contrast, individual orientation determination methods based on dynamical electron beam interaction with a sample provide highly accurate routine orientations (e.g. ±0.05°, Heilmann *et al.* 1982). In transmission electron microscopy (TEM) it is the kikuchi pattern, whilst in the scanning electron microscope (SEM) it is either the electron channelling pattern (ECP) generated by a scanning beam or the electron backscattered pattern (EBSP) generated by a stationary beam, which have been routinely used over the last 10 years in material science. These techniques can be applied to any mineral system including opaques. However, TEM can only be applied to very small regions (less than 3 mm in diameter) and hence small grain sizes (less than 10 μm), which limit its application to micro-textures such as shear bands. Nevertheless, it has been successfully applied to a range of minerals (e.g. plagioclase, Fitz Gerald *et al.* 1983; quartz, Gapais & White 1982). The SEM has the advantage that it can study the surface region of samples of several square centimetres from the centimetre to the micron scale (e.g. Lloyd *et al.* 1992). Orientation determinations can be made from regions of 2–3 μm diameter in ECP-mode and 0.5 μm diameter in EBSP mode with the best commercial systems. In addition to orientation determination, an SEM imaging mode called orientation contrast (OC) is also available with the EC configuration. Regions with the same Bragg orientation with respect to the scanning beam have the same backscattered electron emission (i.e. grey level) in the image. This provides a valuable micro structural image similar to that produced by strain features in the optical microscope with crossed polarizers (e.g. White 1973).

In the presentation that follows we illustrate the important advantages of individual measurement techniques over the traditional texture goniometry. We use an SEM study of two deformed quartzites as examples of the information that can be obtained by the routine measurement of ECPs in a commercially available SEM (CamScan series 4MD).

THE ORIENTATION DISTRIBUTION FUNCTION

Texture measurements made by individual orientation determinations involve the correlation of several symmetry elements of the individual crystal (e.g. optical axes, cleavages, electron channelling bands, zone axes, etc.), which define the complete orientation of the crystal. Certain types of observation (e.g. kinematic electron diffraction, optical axes) are not capable of distinguishing between positive and negative crystal directions, hence the crystals appear to be centric or have Laue symmetry. However, if three or more crystal directions (e.g. zone axes) can be measured, then the complete orientation determination can be unequivocally defined for centrosymmetric crystals (Wenk *et al.* 1988). The situation is more complex for non-centric enantiomorphic crystals, such as quartz, where additional information is required to determine the handedness. The ODF can then be determined, within the limitations of the uniqueness of the individual orientation determination, by the summation of the volume of each individual orientation.

The situation is very different when pole figures measured by X-ray or neutron diffraction are used for texture analysis. The intensity at a given orientation in the pole figure is proportional to the volume of material in the Bragg orientation for diffraction. As stated by Friedel's law, the diffraction intensity for planes $(h\,k\,l)$ and $(\bar{h}\,\bar{k}\,\bar{l})$ is the same because a centre of symmetry is imposed by the diffraction process. The crystal symmetry is therefore increased to an experimental diffraction or Laue symmetry in the kinematic approximation, where dynamic processes such as absorption are ignored. Hence, the sign of a crystallographic direction (for example +**a** axis in quartz) cannot be determined by diffraction. More fundamentally, there is no direct correlation between the orientation of one pole and another pole as the figures are measured independently. The result of the loss of correlation between poles in the pole figure inversion method is that part of the ODF, sometimes called the undetermined part, which remains undefined by pole figure measurement. Formally, in terms of the harmonic analysis, we can identify the measurable part of the ODF f(**g**) by pole figure inversion as the even terms $f(\mathbf{g})^{even}$ and the undetermined part as the odd terms $f(\mathbf{g})^{odd}$,

$$f(\mathbf{g}) = f(\mathbf{g})^{even} + f(\mathbf{g})^{odd} \geq 0, \qquad (1)$$

where **g** is the orientation of each crystal element, described by three Euler angles ψ_1, ϕ, ψ_2 which define the relative orientation of the crystal with respect to a right-handed specimen co-ordinate frame.

Physically it is obvious that the function f(**g**) is always positive, and various methods have been developed to estimate the odd function based on this inequality and other imposed constraints (e.g. Matthies 1979, Matthies & Vinel 1982, Schaeben 1988; see review in Wenk *et al.* 1988). For the evaluation of many physical mineral and/or rock properties the lack of

knowledge of the odd function is not a handicap because all centrosymmetric properties can be derived from the even function as determined by X-ray texture goniometry. These include the majority of the second- and fourth-order tensorial properties of geophysical interest (e.g. magnetic susceptibility, electrical conductivity, thermal expansion, thermal conductivity, elastic and seismic properties). However, two non-centrosymmetric properties in quartz (piezoelectricity and plasticity) do require a knowledge of the function f(**g**) and hence the odd part.

The piezoelectric properties are probably of minor geological interest, although of great commercial interest for electrical components. Quartz is piezoelectric because it has no centre of symmetry, hence the +**a** direction is physically distinct from −**a** direction. Thus, two space groups are required to describe the right- and left-handed forms of α-quartz.

Plasticity also has directional properties, which are polar even in centrosymmetric crystals. For example, the ease of dislocation glide or critical resolved shear stress (CRSS) in a positive direction is not generally equal to that in a negative direction. According to Buerger (1930), the CRSS should be equal for both senses of slip only in the following cases: (1) when there is an even-fold symmetry axis parallel to the slip direction or normal to the slip plane; and (2) when there is a reflection plane normal to the slip direction or parallel to the slip plane. For example, in the case of deformation twinning, the partial twinning dislocation can only glide in one direction. In higher symmetry crystal classes we can expect the polarity of glide systems to be less prevalent, although examples exist in body centred cubic metals. In lower symmetry crystal classes, which includes most rock-forming minerals, the polarity of glide systems will be more common, although documented examples are surprisingly rare (this may reflect a lack of experimental information) and include: calcite $\mathbf{r}^+$ $\{10\bar{1}4\}\langle\bar{2}021\rangle$; dolomite $\mathbf{f}^-$ $\{\bar{1}012\}\langle 02\bar{2}\bar{1}\rangle$; anhydrite $\{012\}\langle 1\bar{2}1\rangle$; and diopside (100)[001] (i.e. sense opposite to twinning).

QUARTZ CRYSTAL STRUCTURE

Enantiomorphism

Low-temperature α-quartz crystallizes in two structural states, either the enantiomorphic right-handed structural helix (space group **P3$_2$22**) or left-handed helix (space group **P3$_1$22**). For texture analysis we can consider these two enantiomorphic forms as separate phases which require independent ODFs of different volume fractions in the aggregate, one for the right-handed form f(**g**)^R and another for the left handed form f(**g**)^L. The simplest case we can imagine is a single crystal which is composed of a right-handed part of orientation $\mathbf{g}^R$ and a left-handed part of orientation $\mathbf{g}^L$. The orientation relationship between the two parts can be described as,

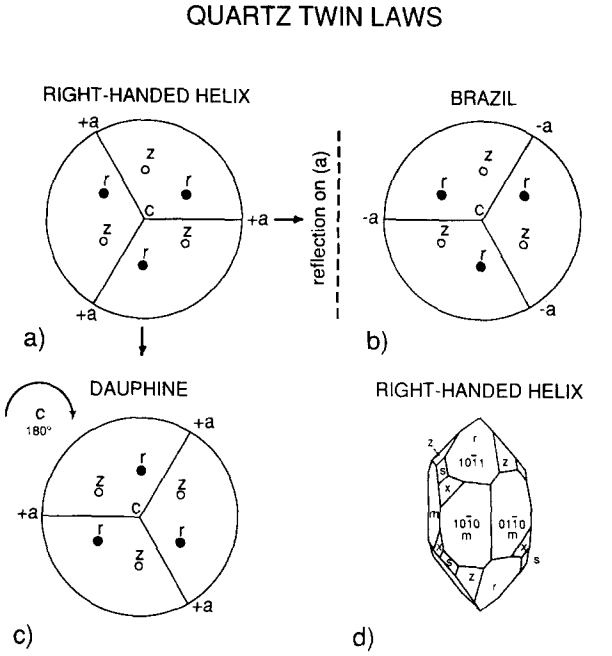

Fig. 1. Quartz axis parallel twin laws. (a) Right-handed structural helix. The positive rhombs **r** are marked with black dot and negative rhombs **z** with an open circle. (b) Left-handed helix in a Brazil orientation with respect to (a). (C) Right-handed structural helix in a Dauphiné twin orientation with respect to (a). (d) Morphology of right-handed structural helix quartz crystal.

$$\mathbf{g}^R = a_{ij} \cdot \mathbf{g}^L, \tag{2}$$

where a_{ij} maps orientation $\mathbf{g}^R$ onto $\mathbf{g}^L$. This operation is a reflection in the $(\bar{1}2\bar{1}0)$ plane (Fig. 1) and is equivalent to the Brazil twin law (see below). In the case where Brazil twinning is an active mechanism during texture development we would predict a cross-relationship between f(**g**)^R and f(**g**)^L. The cross-related ODFs would have the same sample (statistical) symmetries with the right and left forms being interchanged for a given sample direction (Bunge & Esling 1985). The poles to the basal (**c**) and rhombohedral (**r**, **z**) planes will be parallel whereas the +**a** and −**a** axes positions will be interchanged for a given sample direction (Fig. 1).

Two possibilities exist for the determination of the right- and left-handed forms. The most routine determination of handedness can be made by using the optical rotatory power to determine the optical helix. To avoid confusion we will follow the terminology suggested by Donnay & Le Page (1978). The quartz structure with the right-handed helix in a right-handed co-ordinate system has laevorotatory power; the plane of polarization is rotated counter-clockwise, as seen when facing the source of light. Conversely, the left-handed helix has dextrorotatory power; the plane of polarization is rotated clockwise. Thus, the hand of the helix and the sign of the rotatory power are not the same. The angle of rotation (α) is proportional to the thickness of the crystal (21° mm^{-1}) and hence thick sections are required for routine measurement. Wenk (1985) has undertaken such measurements using two coarse-grained quartzites to avoid grain overlap in sections of 0.5 mm thickness. The results showed a very similar distribution of **c** axes for right- and left-handed forms. As the technique is optical,

no information could be obtained about the other crystal axes.

An alternative approach is to use electron diffraction to determine the orientation and handedness. Kikuchi (Faivre & Le Goff 1979) and convergent beam diffraction patterns (Goodman & Johnston 1977, Goodman & Secomb 1977) can be used for enantiomorphic space group determination in TEM. Similarly, the breakdown of Friedel's law has been used in electron channelling patterns (Marthinsen & Høier 1988) for enantiomorphic space group determination. It is clear that ECPs are better suited to routine texture analysis than TEM techniques. The breakdown of Friedel's law in quartz can only be observed for channelling bands which are not parallel to one of the two-fold **a** axes. In Miller–Bravais notation, all bands with one of their three first indices equal to zero are eliminated from the analysis; this includes $(0kil)$, $(h0il)$, $(hk0l)$ and $(000l)$. The determination requires that positive and negative $(hkil)$ channelling bands have different intensities. However, the noise level in the ECPs is such that it may not be routinely possible to determine handedness with this method, especially in highly deformed specimens (see also Olesen & Schmidt 1990).

Textural implications

What bearing do full orientation determination have on the interpretation of texture in terms of the major orienting processes in α-quartz? Texture development will be affected by twinning, dislocation slip and grain boundary migration processes. We now consider repercussions of these mechanisms on texture measurement.

(a) *Twinning.* In α-quartz, two twin laws, Brazil and Dauphiné, are commonly developed either as growth or mechanical defects. The Brazil twin law is a reflection on the **a** $(\bar{1}2\bar{1}0)$ plane. Although, the host and the twin have opposite hands, crystallographic planes remain parallel (i.e. the positive rhombs are parallel), but the piezoelectric sign of the **a** axes changes from the right-handed to left-handed structure (i.e. the $+$**a** axis in the twin will be parallel to the $+$**a** axis in the host, Fig. 1). Brazil twins can be observed by X-ray topography, transmission optical and electron microscopy (e.g. McLaren & Pitkethly 1982). The observations are made using the interference fringe contrast effects due to the phase angle between the right and left structures and the presence of a fault vector parallel to the composition plane. Thus, it is fringes located at the boundary rather than orientation dependent contrast between host and twin that are observed. The physics of the observation are important because it is evident that such twins cannot be detected in SEM using the interference contrast of back scattered electrons from a solid specimen because the electrons are back scattered only from the surface region (<50 nm). Brazil twins nucleate during growth and hence could nucleate during grain boundary migration as growth accidents. Mechanical Brazil twins have also been produced in experimental deformation of natural single crystals at high stresses where the twin is associated with the development of glass on basal planes. It would therefore appear that mechanical Brazil twins are unlikely to be active in natural deformation at low stresses.

Dauphiné twins may be described as 180° rotation about the **c** axis, which is equivalent to a 60° rotation as the **c** axis is a three-fold axis. Both the host and the twin have the same structure, either left- or right-handed, and the positive piezoelectric $+$**a** axis in the host is parallel to the negative $-$**a** axis in the twin (Fig. 1). If the host and twins have equal volumes then the piezoelectric effect will cancel for the grain in question. The twins cannot be observed optically as the **c** axis in the twin and host are parallel. In the SEM, TEM and X-ray topography Dauphiné twins are routinely observed because strongly diffracting planes with different reflecting powers (or structure factors) are parallel. For example, whilst the positive rhomb **r** in the host is parallel to the negative rhomb **z** in the twin, the intensity diffracted by **r** is greater than **z** and hence the regions in the host and twin orientations can easily be imaged in SEM, TEM or X-ray topography using the appropriate diffracting conditions. In this case it is the orientation dependent contrast between the host and the twin that is observed. At this point it should be recalled that X-ray and neutron texture goniometry can also contribute to our understanding of Dauphiné twinning. Although in diffraction based pole figure measurements one can only measure the combined pole figure **r** + **z** as they have the same Bragg angle, the data processing methods (e.g. harmonic analysis) are capable of calculating separated **r** and **z** pole figures. Dauphiné twins develop during growth, for example during the phase transition $\beta \rightarrow \alpha$ quartz and during deformation. Although no deformation of the structure is caused by Dauphiné twinning (but see Lloyd *et al.* 1992) it has been found experimentally in quartzites (e.g. Tullis *et al.* 1973) that differential stress activates Dauphiné twinning resulting in a preferred orientation of the pole to **r** rhombs parallel to the compressional stress axis.

(b) *Dislocation slip.* Perhaps the most important orienting mechanism, at least in α-quartz tectonites, is dislocation slip (e.g. Christie & Ardell 1976, Wenk & Christie 1991). Because slip is centrosymmetric, we can therefore consider α-quartz to belong to point group 32/m rather than point group 32 (e.g Lister *et al.* 1978). In so doing, we can avoid the need to determine the right- and left-handed forms as we have implicitly assumed a centre of symmetry for slip. The same is also true for Dauphiné twinning as there is no need to distinguish the handedness of the host and twin, but not for Brazil twinning (see above).

(c) *Grain boundary migration.* This process is much less well understood from all points of view than those considered previously. Nevertheless, it is clear that grain boundary migration can have a profound effect on the crystallographic textures of an aggregate because large

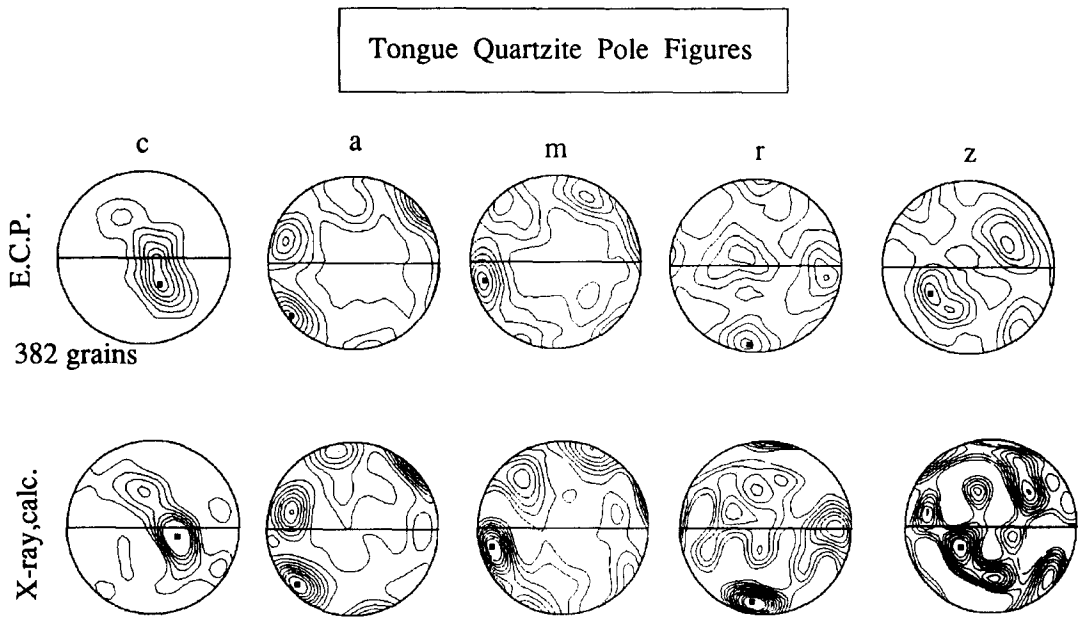

Fig. 2. Calculated pole figures from the ODF coefficients from Tongue quartzite, contoured in multiples of a uniform distribution (m.u.d.). Harmonic expansion of the pole figure coefficients truncated at $L = 22$ for the ECP data and $L = 8$ for the X-ray data. Lineation E–W, foliation vertical.

volume fractions can attain similar orientations by this process (e.g. Jessell 1986, Urai *et al.* 1986, Wenk & Christie 1991). Migration may favour the development of grains with the same handedness. The few scattered observations available suggest that this may be the case (Frondel 1978) and hence we need to be able to determine the handedness to characterize fully the mechanism(s) of grain boundary migration.

The driving force for migration may be derived from the spatial variation of the stored elastic strain energy due to heterogeneous dislocation density. The dislocation density will vary as a function of relative orientation of crystals with respect to the deviatoric (local) stress and the relative efficiency of recovery processes such as climb, annihilation and cross-slip for the slip system under consideration. We must also consider possible chemical driving forces (e.g. point defect concentrations for quartz). Finally, there is the driving force for the minimization of the overall grain boundary energy. This may simply reduce the curvature of the boundary, but perhaps more fundamentally for texture analysis is the elimination of arbitrary grain boundaries by the preferential preservation of low energy boundaries (e.g. twin orientations). The sub-grain rotational recrystallization of quartz will be strongly linked to the dislocation slip system and will produce grain boundaries of rather specific crystallographic orientations (e.g. former sub-grain boundaries).

QUARTZ TEXTURE ANALYSIS

Bulk texture analysis of quartzites

The orientation of single grains in Tongue quartzite (Moine Thrust zone, Eriboll, N. Scotland) has been measured using ECPs. In a previous study (Lloyd *et al.* 1987), 100 grains were measured and indexed using an electron channelling map for quartz constructed over a spherical surface (Lloyd & Ferguson 1986). An additional 282 grains have been measured and all ECPs indexed using a computer indexing program (*CHANNEL*, Schmidt & Olesen 1989). The 382 individual orientations have been indexed as right-handed crystals with convention that the positive rhomb **r** is a stronger reflection than the negative rhomb **z** (see Donney & Le Page 1978). We have used the method of Wagner *et al.* (1981) to calculate the coefficients C_L^{mn} of the spherical harmonic method, which provides an analytical expression of the total ODF f(**g**). The harmonic method allows a straightforward calculation of crystal pole figures, inverse pole figures, physical properties and a comparison with X-ray texture goniometry via the even part of the total function.

For comparison, the pole figures for **a**, **m** and **r** + **z** have been measured on the same specimen using an X-ray texture goniometer and recalculated from the even coefficients with an $L_{max} = 8$ (Lloyd *et al.* 1987). The ECP and X-ray calculated pole figures have similar density distributions (Fig. 2), indicating that the ECP method has statistically sampled the texture. The ECP pole figures have a stronger coherence or single-crystal like pattern than the X-ray pole figures. The ECP requires that the orientations of several planes (channelling bands) are measured for each crystal orientation, whereas in the X-ray method each pole figure is measured independently. The difference in the two techniques is clearly revealed in the lower coherence of the X-ray harmonic coefficients which were themselves determined with the crystal symmetry properties imposed by the quartz structure. The reduced correlation between pole figures in X-ray measurements is

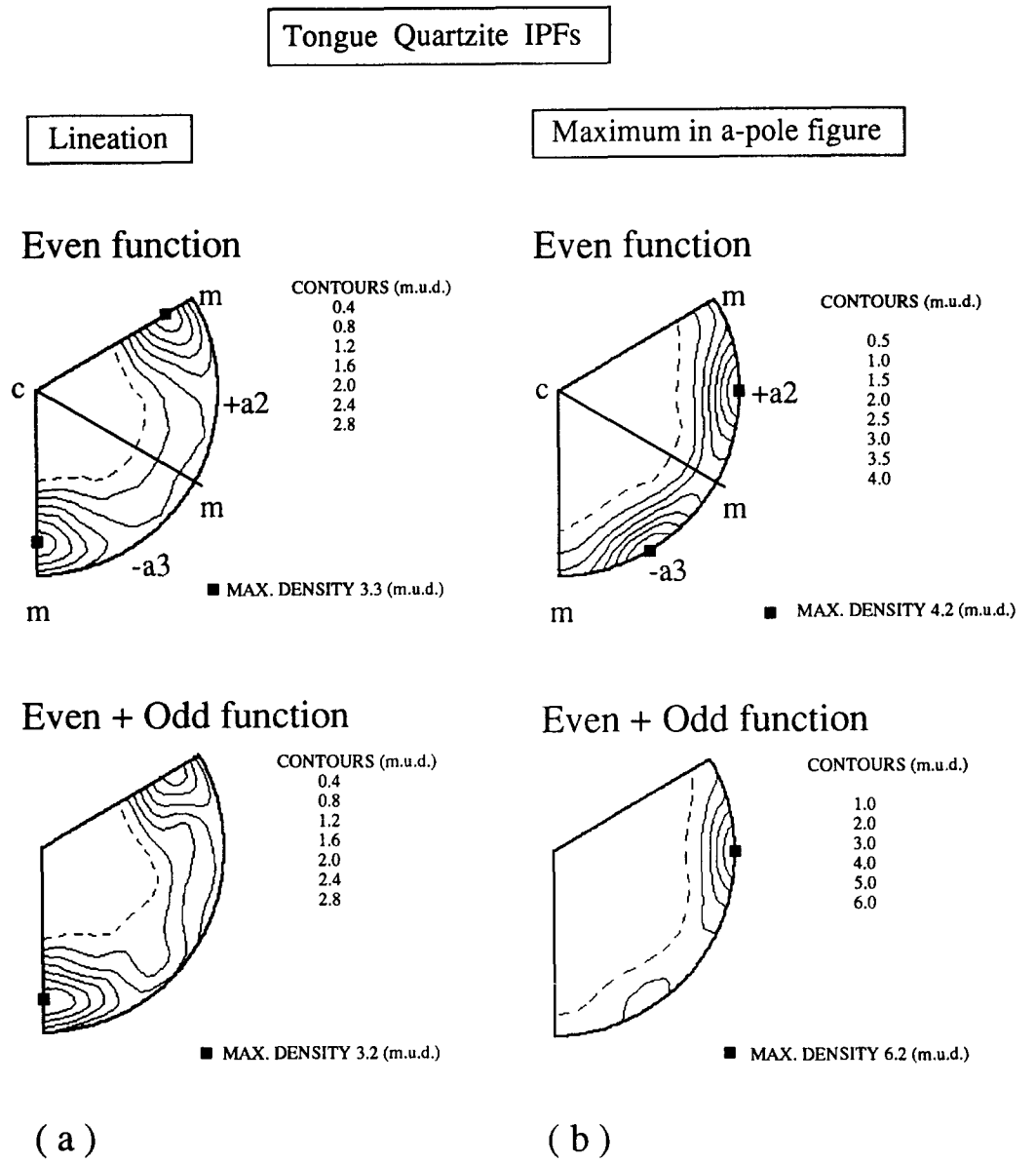

Fig. 3. Inverse pole figures calculated from the ECP coefficients ($L = 22$) for Tongue quartzite, for the directions parallel to the lineation (X) and the maximum in **a** pole figure. Minimum contour is a dashed line.

probably due to experimental factors which vary from pole figures to pole figure, such as absorption corrections.

Inverse pole figures (IPF) have been calculated from even and even + odd coefficients derived from the ECP data. We have chosen to illustrate the symmetry of the IPFs with two directions. Firstly, parallel to the lineation (Fig. 3) the IPF calculated from the even coefficients has a mirror symmetry about the **c** − **m** line (an **a** plane). In the IPF calculated with even + odd coefficients (i.e. the total function) a slight asymmetry is evident about the **c** − **m** line. The major feature of both IPFs is a strong concentration of lineation directions close to the **m** direction. The second direction we have chosen is the maximum in the **a** pole figure. Again the IPF calculated from the even coefficients has mirror symmetry about **c** − **m** and the IPF calculated from the even + odd coefficients has an asymmetry about **c** − **m** line. In this case, the asymmetry is extremely marked with maximum of over six parallel to $+\mathbf{a}_2$ and two parallel to $-\mathbf{a}_3$. Note the signs of the **a** axes ($\mathbf{a}_2$, $\mathbf{a}_3$) must be different in the IPF, but their signs are arbitrary in terms of physical properties, such as piezoelectricity, because we have not determined the handedness of the crystals. The IPF is illustrating that the pole figures, such as **a**, are not revealing the full nature of the texture as the $+\mathbf{a}$ and $-\mathbf{a}$ poles (or directions) have not been distinguished in the $\pm\mathbf{a}$ pole figure representation.

The ODF can be represented as a series of serial sections at constant values of the Euler angle ψ_1. In Fig. 4 we present the sections for the even and total (even + odd) functions. The symmetry of the two functions is very similar, there are no major peaks in the even function that do not appear in total function, although there are sometimes minor peaks referred to as ghosts (e.g. Matthies & Vinel 1982). However, the peaks in the total function are significantly higher than in even function. For example, the prominent peak at $\psi_1 = 120°$ section is 13.2 in the even and 19.6 in the total function. The even function has significant volumes of physically

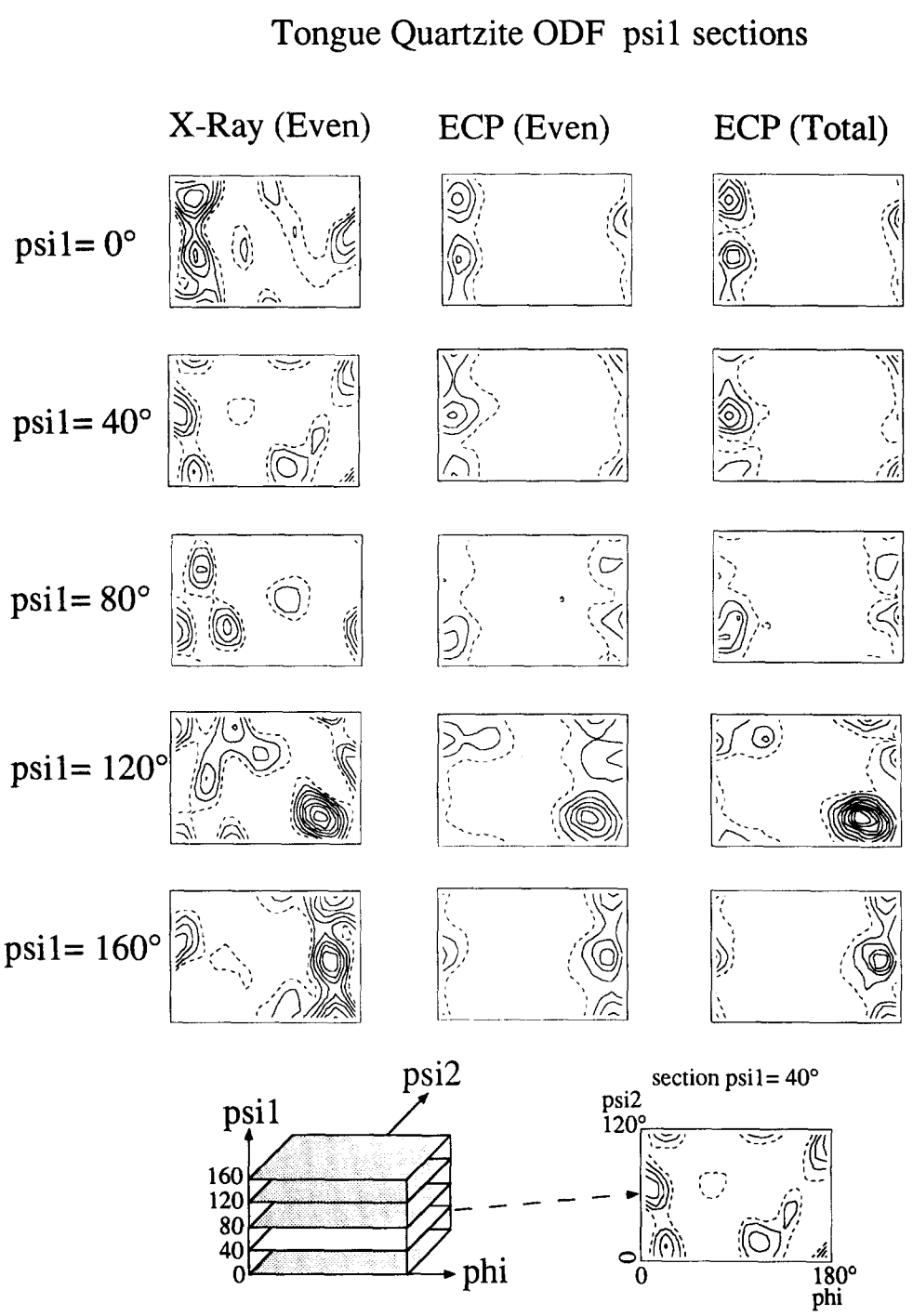

Fig. 4. Sections of the three-dimensional ODF with orthogonal axes ψ_1, ϕ and ψ_2. ODF sections at constant ψ_1 with an interval of 40° for Tongue quartzite. Even function for X-ray and ECP data. Total (even + odd) function for the ECP data. Calculated with truncation at $L = 8$ for X-rays and $L = 22$ for ECPs. Contours at 2 m.u.d. intervals. The lowest contour (2 m.u.d.) is a dashed line.

meaningless negative values, whereas the total function is always zero or positive.

Local texture analysis of quartzites

Individual orientation measurements provide a statistical estimate of the texture of a polycrystal in a similar manner to X-ray texture goniometry. The number of measurements required depends upon the nature of the texture itself. In the extreme case of a single crystal only one measurement is required, whereas for a random texture a very large number of measurements may be necessary depending on the sampling procedure. When the measurements are made grain-by-grain we have also a spatial measure of texture which can be allied with micro structural observations (e.g. combination of ECP measurements and OC images). We therefore have information of the relative orientation or misorientation between neighbours (either grains or subgrains) and their spatial distribution.

We can describe the misorientation (or rotation) Δg_{ij} between two volume elements of orientation $\mathbf{g}_i$ and $\mathbf{g}_j$ which brings the two orientations into coincidence by $\Delta g_{ij} = \mathbf{g}_j^{-1} \cdot \mathbf{g}_i$. These three orientations may be de-

scribed in terms of Euler angles, rotation matrices or axis–angle pairs. Such an approach evaluates the three degrees of freedom associated with the rotation which brings the two crystal lattices into perfect registry, but does not define the orientation of their (planar) interface (an additional two degrees of freedom involved), nor the rigid body translation necessary (three degrees of freedom) for the complete macroscopic characterization of an interface between two crystals (Smith 1975). Bearing in mind that we have only partially characterized the interface between crystals with measurements of Δg_{ij}, it is clear that such information will help to further constrain the interpretation of the mechanisms of texture development, as the following examples illustrate.

Example (1). In the case of dislocation glide, low-angle subgrains boundaries (sgb) are produced in order to reduce the stored elastic strain energy. The rotation at a planar sgb between two sub-grains is given by Frank's relation,

$$\mathbf{d} = \Sigma \mathbf{b}_i = (\mathbf{r} \wedge \mathbf{u}) 2 \sin \theta/2, \qquad (3)$$

where $\mathbf{r}$ is an arbitrary line in the plane of the sgb, $\mathbf{d}$ is the vector sum of the Burgers vectors $\mathbf{b}_i$ of all the dislocations by $\mathbf{r}$, $\mathbf{u}$ is a unit vector parallel to the axis of rotation, and θ is the rotation angle. This approach has been applied to glide systems in quartz by Trépied *et al.* (1980) and Mainprice *et al.* (1986). In a quartzofeldspathic shear zone in Lewisian gneiss, hereafter called Torridon 'quartzite', Lloyd *et al.* (1992) studied the local quartz texture as a function of strain along a transect of the shear zone. In a region on the edge of a shear zone (shear strain ≈ 1), in the core of a grain the misorientation between subgrains was measured by SEM/ECP. The misorientation axes in structural co-ordinates for subgrains 58 and 60 is close to the Y axis (Figs. 5a and 6a). In crystallographic co-ordinates the rotation axis is $[\overline{1.34}\ 0.01\ 1.33\ 0.19]$ and the angle of 13.13°, close to the $[\bar{1}010]$. Such a misorientation could have been produced by slip on $\langle \mathbf{a}_1 \rangle (\mathbf{c})$ forming a pure tilt subgrain wall. Furthermore, the rotation angle in theory gives us an estimate of dislocation density in subgrain wall, at least at low values of θ. However further analysis of the local texture in this region shows the situation to be more complex. The mosaic of subgrains around 58 and 60 show a dispersion of orientations in structural co-ordinates (Fig. 7a) and a scatter of orientation of the misorientation axes in structural and crystallographic co-ordinates (Figs. 7b & c). To assess if this complexity is typical, we have studied the local texture in the adjacent grain which has a core and mantle structure. The mosaic of subgrains which constitute the core has more marked dispersion trails in structural co-ordinates (Fig. 8a) with an apparent rotation about the intermediate structural axis, Y. The misorientation axes are again scattered in orientation (Figs. 8b & c). The mantle subgrains show very marked dispersion trails (Fig. 9a) with a rotation about Y or perhaps about the **r** rhomb. The misorientation axes again show considerable dispersion in structural and crystallographic co-ordinates (Figs. 9b & c).

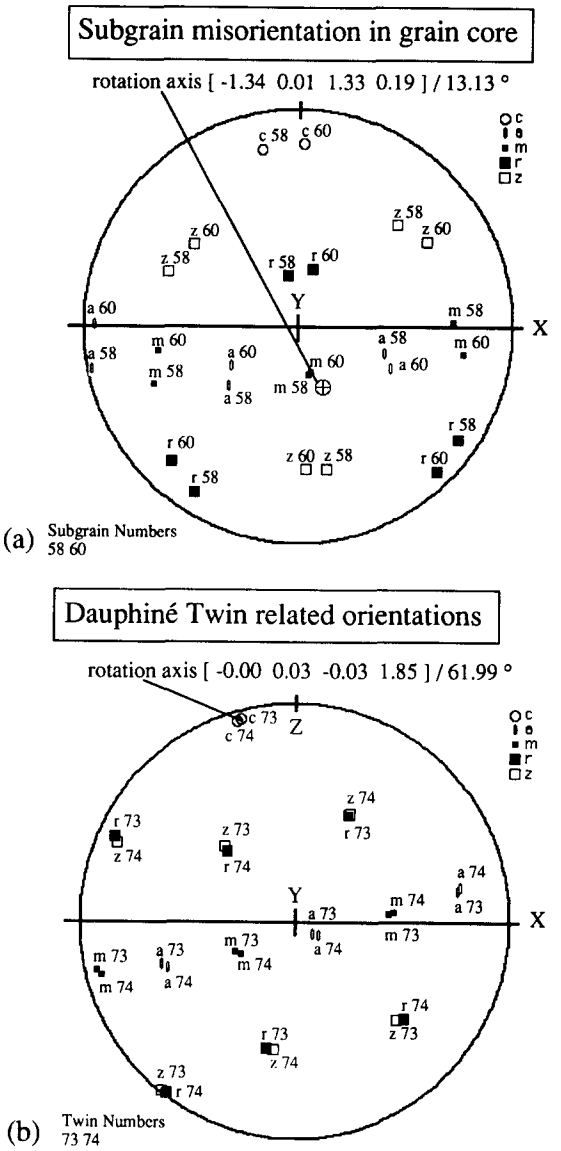

Fig. 5. Examples of misorientation analysis in Torridon 'quartzite'. (a) Subgrain misorientation between subgrains 58 and 60. (b) Twin misorientation between grains 73 and 74.

Example (2). Similarly, for twinning we can measure the rotation axis and angle to deduce the twin law. In the case of the **c** axis parallel twins, it is only possible to determine the Dauphiné law as the **r** and **z** forms are parallel in the host and twin, respectively. For example, grains 73 and 74 in Figs. 5(b) and 6(b) have misorientation axis $[0.00\ 0.03\ \overline{0.03}\ 1.85]$ and angle of 61.99°, close to the ideal values of [0001] and 60° for the Dauphiné twin law. Inclined axis twin laws are rare in α-quartz (Frondel 1962), although a crystallographic study by McLaren (1986) has shown that such relative orientations have coincidence site lattice (CSL) periodicities which are probably associated with low energy grain boundary structures. In a CSL orientation the fraction of lattice points of two crystals that are in coincidence is given as $1/\Sigma$. In trigonal crystals, such as quartz and calcite, rotations about the **c** axis of 60.00°, 38.21°, 27.80°, 46.83° and 21.79° produce CSLs with Σ of 3, 7, 13, 19 and 21, respectively (McLaren 1986, Grimmer 1989, 1990). The Dauphiné twin law is a CSL orientation

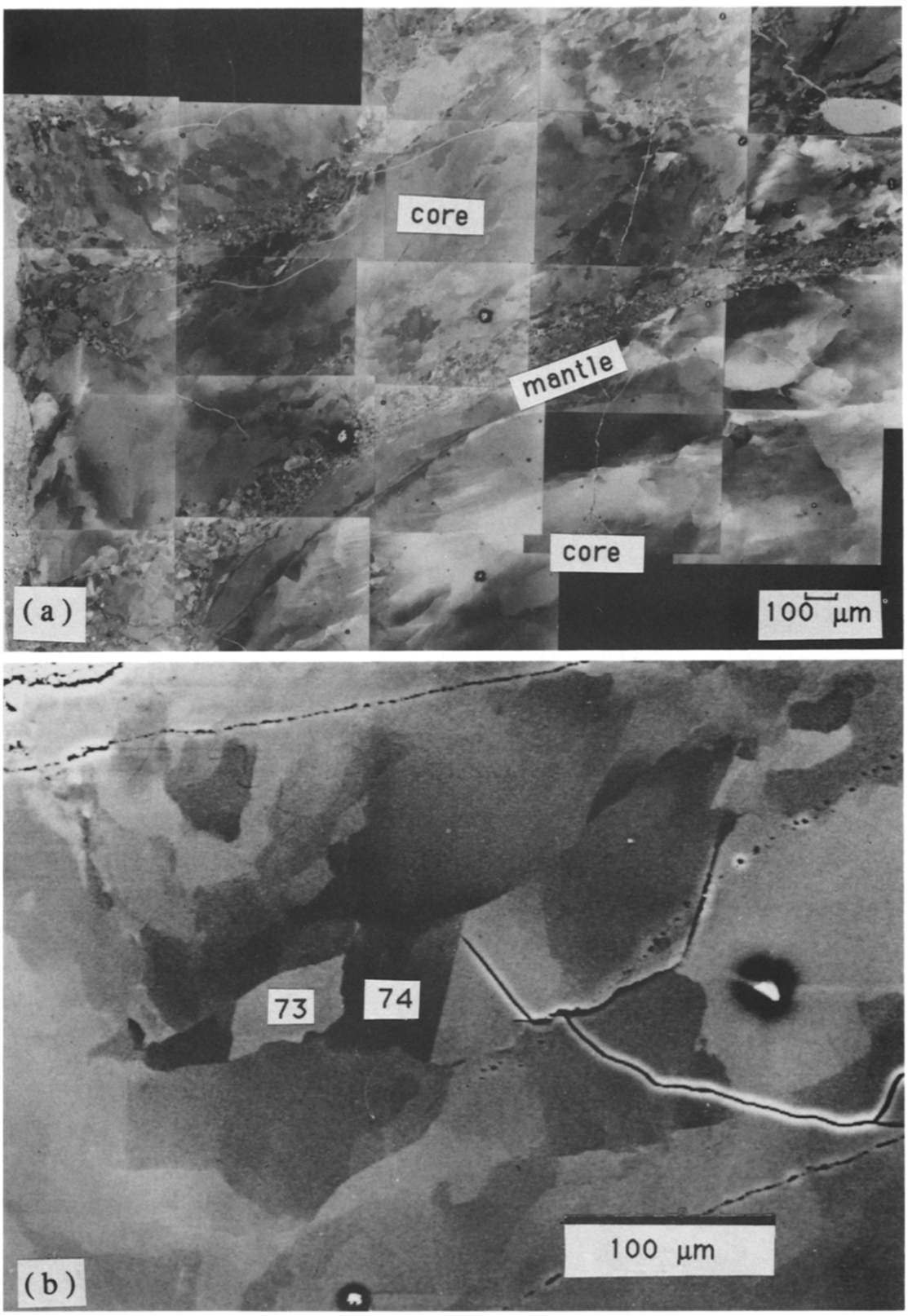

Fig. 6. Orientation contrast SEM images of Torridon 'quartzite'. (a) Mosaic of subgrains with core and mantle structure. Subgrains 58 and 60 of Figs. 5(a) and 7 are located in the upper core region. The core and mantle subgrains of Figs. 8 and 9 are the lower grains marked core and mantle. (b) Dauphiné twins and the location of 73 and 74 in Fig. 5.

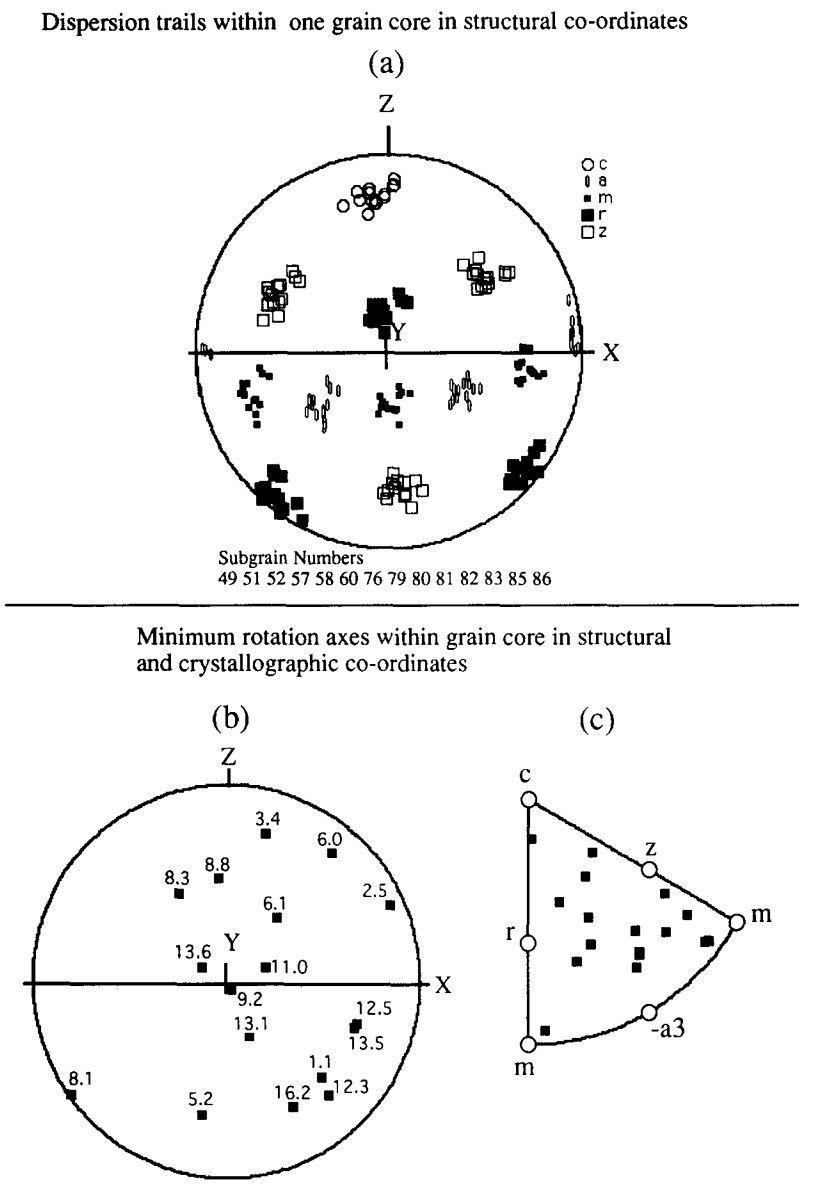

Fig. 7. Misorientation analysis of subgrain mosaic in Fig. 6(a). (a) Dispersion trails in grain core in structural co-ordinates. (b) Misorientation axes of subgrains in structural co-ordinates. (c) Misorientation axes of subgrains in crystallographic co-ordinates. Note we use the 60° sector for bicrystal misorientation axes, rather than 120° sector used for the IPFs in Fig. 3. Square symbols are the misorientation axes. The numbers at each data point in (b) are the misorientation angles.

with $\Sigma = 3$. In any mineral a CSL will be produced by a rotation about any crystallographic direction $[uvw]$ which is exactly normal to a plane (hkl) with the same indices, i.e. $[uvw]$ is parallel to $\perp(hkl)$. In the case of quartz, a rotation about the **c** axis or any direction perpendicular to **c** in the basal plane, will produce CSLs.

Example (3). All twin orientations (180° rotations) produce CSLs but other orientation relationships may also produce CSLs. The presence or absence of such interface structures is likely to be important for grain boundary migration and grain boundary sliding mechanisms. The existence of epitaxial relationships between crystals of different symmetry (and chemistry) indicate that the periodicity of interface structure may be important even in polyphase rocks. In metamorphic processes phase changes can produce distinct crystallographic orientation relationships between phases (Mainprice *et al.* 1990). For example, in the case of andalusite to silliminite transformation in a granite aureole the **b** axes are parallel (Lloyd *et al.* 1991). From a geometrical point of view CSLs will be less frequent as the crystal symmetry decreases. However, decreasing symmetry often results in more anisotropic physical properties and hence perhaps an increasing importance of such interfaces. To date, few measurements are available on ceramic or geological materials (e.g. McLaren 1986) to evaluate the importance of periodic interface structures in rocks.

To understand the physical significance of a misorientation measurement, it is often essential to generate all the symmetrical equivalent misorientations of an experimental determination. For each experimentally indexed orientation (**g**) there are n symmetry equivalent orien-

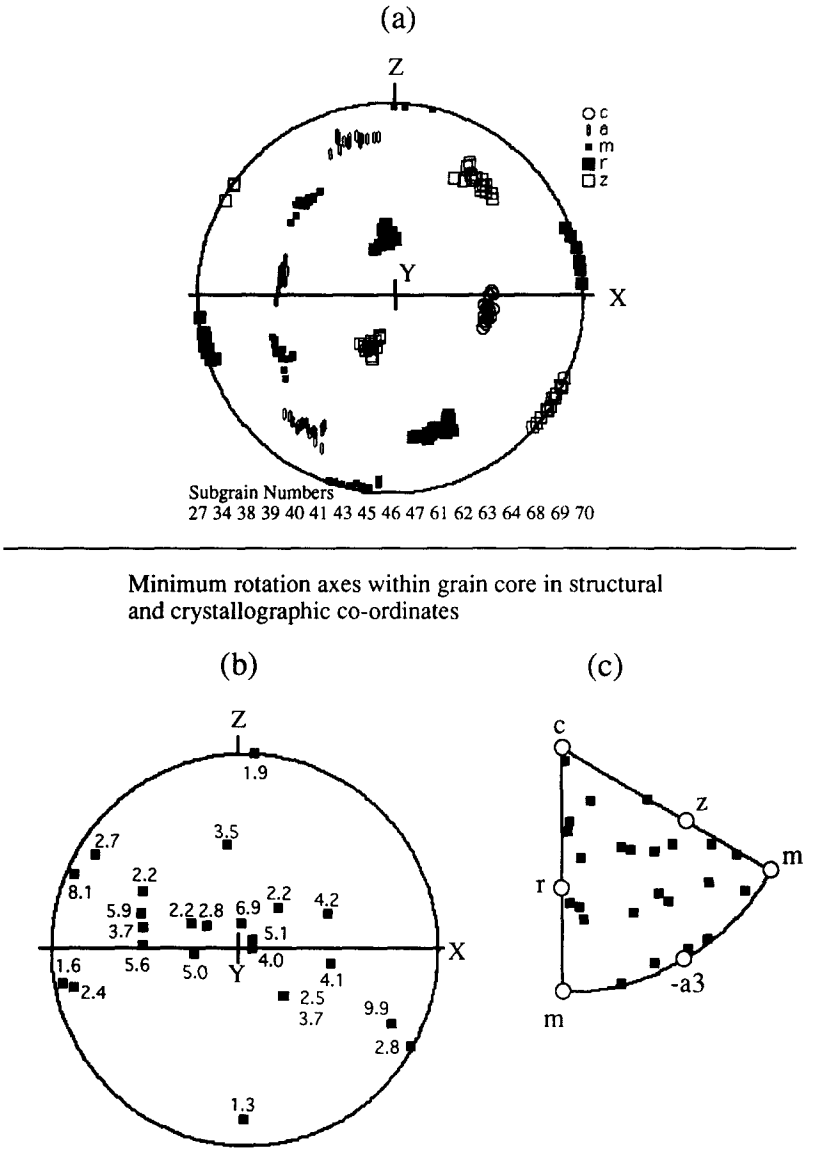

Fig. 8. Misorientation analysis of subgrains grain core in Fig. 6(a). (a) Dispersion trains in grain core in structural co-ordinates. (b) Misorientation axes of subgrains in structural co-ordinates. (c) Misorientation axes of subgrains in crystallographic co-ordinates. Square symbols are the misorientation axes. The numbers at each data point in (b) are the misorientation angles.

tations. If we have n symmetry operations for the crystal symmetry given in matrix form as S^n, then there are n^2 symmetry equivalent misorientations Δg^n_{ij} and Δg^n_{ji}

$$\text{and} \qquad \Delta g^n_{ij} = (S^n \cdot \mathbf{g}_j)^{-1}(S^n \cdot \mathbf{g}_i) \qquad (4)$$
$$\Delta g^n_{ji} = (S^n \cdot \mathbf{g}_i)^{-1}(S^n \cdot \mathbf{g}_j).$$

For α-quartz, we have $n = 6$ symmetry equivalent orientations for each crystal ($\mathbf{g}_i$ and $\mathbf{g}_j$) and hence $n^2 = 36$ symmetry equivalent misorientations Δg^n_{ij} and Δg^n_{ji}. Δg^n_{ij} is the operation that rotates orientation $\mathbf{g}_i$ into perfect coincidence with orientation $\mathbf{g}_j$ and Δg^n_{ji} is the operation that rotates orientation $\mathbf{g}_j$ into perfect coincidence with orientation $\mathbf{g}_i$. Δg^n_{ji} is the transpose matrix of Δg^n_{ij} as rotation matrices are orthogonal. Both Δg^n_{ij} and Δg^n_{ji} are required for the description of a bicrystal as we have arbitrarily assigned the orientations of the two crystals the labels i and j; these labels may be exchanged in equation (4) to give Δg^n_{ji} and Δg^n_{ij}. For the complete description of a bicrystal composed of two holohedral trigonal crystals there are $2n^2 = 72$ symmetry equivalent misorientations (Grimmer 1980). One may choose any one of the 72 degenerate misorientations as they are physically indistinguishable from the orientation measurement. In practice a choice is made according to the application: (a) low-angle boundaries (or sub-boundaries)—smallest rotation angle; (b) twin description—180° rotation angle; (c) periodic interface or CSL—tabulated axis–angle pair; and (d) Euler angles—texture analysis.

In the same way that we can describe the ODF of crystal orientations in sample co-ordinates we can describe the misorientation ODF (MODF) in crystal co-ordinates (e.g. Pospiech *et al.* 1986, Bunge & Weiland

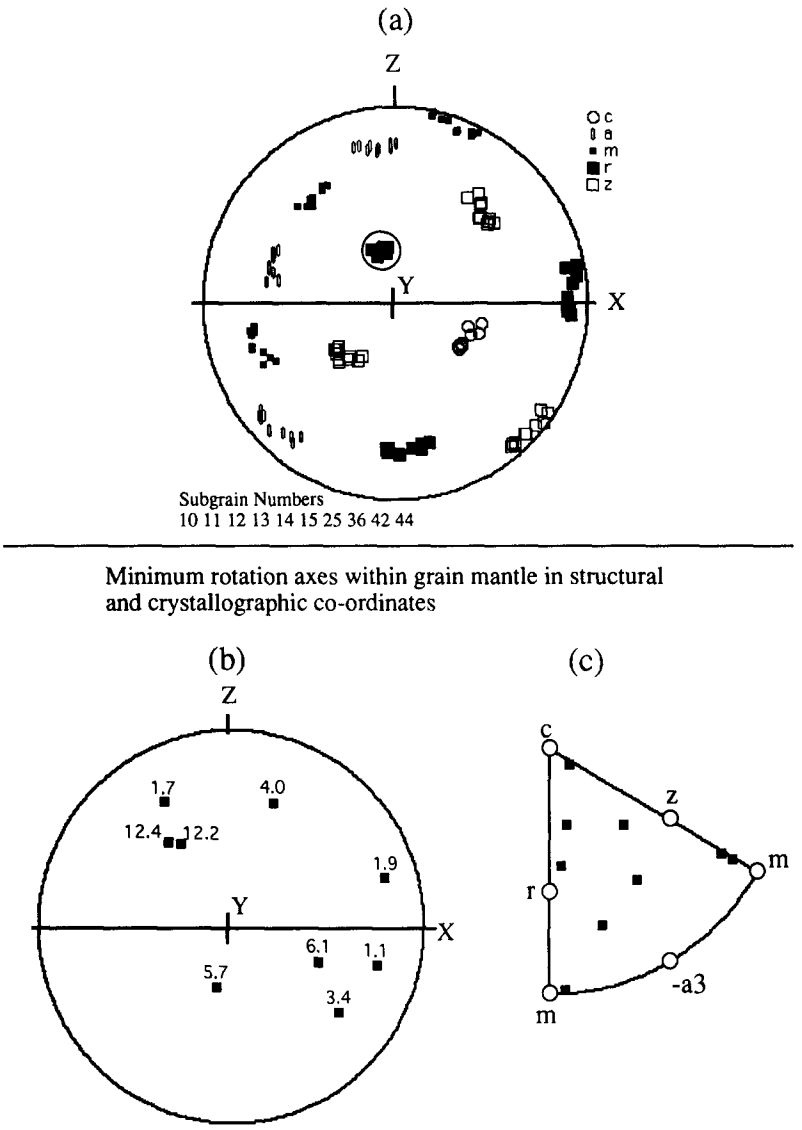

Fig. 9. Misorientation analysis of subgrains grain mantle in Fig. 6(a). (a) Dispersion trails in grain mantle in structural co-ordinates. Note tight grouping of positive rhombs **r** near *Y*, marked by circle. (b) Misorientation axes of subgrains in structural co-ordinates. (c) Misorientation axes of subgrains in crystallographic co-ordinates. Square symbols are the misorientation axes. The numbers at each data point in (b) are the misorientation angles.

1988, Adams & Field 1992) between grains which one can characterize by distributions $f^a(g)$ and $f^b(\Delta g \cdot g)$. Three such distributions can be described.

(1) An uncorrelated $[F_{\text{uncorr}}(\Delta g)]$ or disordered MODF,

$$F_{\text{uncorr}}(\Delta g) = \int f^a(g) \cdot f^b(\Delta g \cdot g)\, dg \qquad (5)$$

which is the autocorrelation of the ODF and represents the misorientation of each orientation with every other orientation regardless of spatial co-ordinates of the two orientations. The uncorrelated MODF can be calculated from ODFs derived from volume diffraction methods (e.g. X-ray or neutron texture goniometry).

(2) The correlated $[F_{\text{corr}}(\Delta g)]$, ordered or physical MODF can be calculated only from individual measurements; in this case only the misorientation between neighbouring orientations are taken into account,

$$F_{\text{corr}}(\Delta g) = \int f^a(g) \cdot f^b(\Delta g \cdot g)\, dg. \qquad (6)$$

(3) A third type of distribution may be derived from the uncorrelated and correlated MODF, which is simply the ratio of two distributions $[F(\Delta g)]$ and which helps to identify the misorientations that are more frequent between neighbours than in all possible situations found in the polycrystal with that specific texture

$$F(\Delta g) = \frac{F_{\text{corr}}(\Delta g)}{F_{\text{uncorr}}(\Delta g)}. \qquad (7)$$

Applications using these functions are developing rapidly in metallurgy (e.g. Field & Adams 1992) and we can expect them to make an important impact in Earth Sciences for grain boundary sensitive properties (e.g. recrystallization, grain boundary transport). However, to use these functions the basic bi-crystal crystallography of minerals needs to be developed to define the appropriate asymmetric domains. For example, Grimmer (1990) suggests that for trigonal materials the asymmet-

ric unit is "a spherical triangle bounded by two mirror planes" and "the plane perpendicular to its three-fold symmetry axis"; i.e. the 60° sector bounded by $\perp(0001)$, $\perp(10\bar{1}0)$ and $\perp(01\bar{1}0)$ which we have used in Figs. 7, 8 and 9.

DETERMINATIONS OF PETROPHYSICAL PROPERTIES

Introduction

Texture data provide a unique possibility for the calculation of anisotropic tensorial properties of rocks. The majority of rock-forming minerals have anisotropic physical properties (e.g. elasticity). It is often difficult or impossible to evaluate such properties in all directions experimentally, whereas it is straightforward to calculate the values from the single crystal tensors and the texture data. As most geologically important properties are centrosymmetric, the calculations only require the even part of the texture function. For many applications volume-true texture measurement by X-ray or neutron goniometry are more appropriate for pure aggregates (e.g. quartzites). However, as most rocks are polyphased, individual measurement techniques have their place.

Electrical conductivity

For studies of electrical conductivity, either by resistivity or magnetotelluric methods, have shown the Earth's crust to be many orders of magnitude more conductive than predicted by laboratory measurements of dry rock samples (e.g. Shankland & Ander 1983). The agreement between field and laboratory measurements is much better for the upper mantle (Shankland 1981). In the crust, high conductivity is associated with high heat flow (e.g. Kaufman & Keller 1981) and hence the *in situ* conductivity mechanism is a thermally activated process. The discrepancy between laboratory and field measurements can be explained by the addition of a small amount of highly conductive material to the insulating silicate rock. Some experimental studies on carefully dried sandstones require the presence of a high dielectric constant grain boundary coating to explain the measurements (Tuck & Stacey 1978). Most workers (e.g. Connernery *et al.* 1980) favour the addition of water. For example, the addition of 1–2% water can increase the sub-solidus electrical conductivity of granite by 4–5 orders of magnitude (Olhoeft 1981). Shankland & Ander (1983) estimate that most lower crustal conductivity measurements can be explained by the presence of 0.01–0.10% water in rocks containing ~0.1% porosity which may or may not be connected. The case of electrical conductivity is an interesting one as the extrinsic effects associated with a second phase (e.g. H_2O) may completely mask the intrinsic ('dry') lattice conductivity. In such a case the intrinsic anisotropic electrical properties we calculate using texture measurements and single crystal values may have no practical value for geophysics. The situation may be different for mantle rock compositions as suggested by Shankland (1981).

Bearing in mind the limitations mentioned above we have calculated the dielectric constant for Tongue quartzite. The calculation procedure for second order properties of an aggregate of N grains of equal volume is as follows. The single crystal tensor property (T_{ij}) is rotated into the grain orientation (T'_{ij}) using the rotation matrix (g_{ij}) defined by the Euler angles,

$$T'_{ij} = g_{ik} \cdot g_{jl} \cdot T_{kl}. \tag{8}$$

The tensor property for each grain (T'_{ij}) are summed to give the Voigt average aggregate property defined by,

$$\bar{T}_{ij}^{\text{Voigt}} = \frac{\sum_{1}^{N} T'_{ij}}{N}. \tag{9}$$

Similar methods are used for the Reuss average. The aggregate tensor property T_{ij} can then be evaluated (T) in any direction (X) by

$$T = T_{ij} \cdot X_i \cdot X_j. \tag{10}$$

The calculated anisotropy of Tongue quartzite is very low (1.3%) because the quartz single crystal anisotropy is itself very low (3.5%). Hence the evaluation of this particular property has no geophysical application, except to indicate that it will be almost isotropic even in a strongly textured pure quartzite. A similar situation exists for magnetic susceptibility. The single crystal has an anisotropy of less than 1%, hence the polycrystal is virtually isotropic.

Thermal conductivity

Thermal conductivity (or thermal diffusion) is an extremely anisotropic property in single crystal quartz. The palaeo-distribution of heat flow will be directly controlled by the anisotropy of the thermal conductivity of rocks. Such distributions can be deduced from metamorphic isograds (Wenk 1970) and K–Ar cooling ages (Borradaile & Hermes 1980) which record the palaeo-isothermal surfaces at a given epoch. Many sophisticated numerical models of complex metamorphic histories have failed to take into account the anisotropy of thermal conductivity, even though it may be as high as a factor of 2 in schists (Wenk & Wenk 1969). Indeed, in some metamorphic root zones where the foliation is nearly vertical, the parallelism of the schistosity and the metamorphic isograds is explained by the high thermal conductivity parallel to the schistosity (Wenk 1970, Den Tex 1975). As with electrical conductivity, the intrinsic thermal conductivity calculated using texture measurements will only be valid in the absence of other heat transport mechanisms, such as fluid migration. In the

case of thermal conductivity an interconnected network of pores or fractures will be necessary for fluid percolation and hence fluid volumes much larger than 0.1% which perturbed the intrinsic electrical conductivity values are required to perturb the thermal conductivity.

The calculated intrinsic thermal conductivity for Tongue quartzite has an anisotropy of 30.1%, with a maximum broadly coincident with the maximum in the **c** axis pole figure. The **c** axis is the axis of greatest thermal conductivity in the single crystal. The apparent coincidence between the minimum in thermal conductivity and the maximum in the **a** axis pole figure is fortuitous. It must be due to the **c** axis distribution, because the second-order tensor properties have a unique value in the basal plane for hexagonal or trigonal crystals.

Thermal expansion

The increase in temperature from some reference value results in anisotropic change in dimensions of a single crystal quartz. In a quartz polycrystal the same temperature increase will result in strain incompatibilities at the grain boundaries. If there is no cohesion on the grain boundaries the polycrystal will disaggregate. In the geological or experimental situation where the aggregate is under confining pressure, the temperature rise will cause the build-up of internal stresses which are proportional to the incompatibility strains. To evaluate the internal stresses rigorously, we need to know the orientation of individual grains and their neighbours. Such information can be obtained from ECPs. On the other hand, if we want to consider the specimen as one volume element (i.e. not considering neighbour interactions), then we can integrate the properties of all grains. We have performed an integral calculation of the thermal expansion of Tongue quartzite. The anisotropy is high at 24.2%. The minimum thermal expansion of a single crystal is parallel to the **c** axis and hence the minimum thermal expansion of a polycrystal is parallel to the maximum in the **c** axis pole figure. If we calculate the Young's modulus (E), we can evaluate the variation of the compressive stress (σ) with direction, using

$$\sigma = \alpha \cdot E \cdot \Delta T, \tag{11}$$

where α is the thermal expansion, ΔT is the change in temperature. We have assumed that the sample is perfectly constrained; i.e. there is no external dimensional change of the aggregate. If the temperature is raised from a reference value, compressive stresses are generated. On the other hand, if the temperature is lowered then tensile stresses result. In the approximation that tractions on the grain boundaries and neighbour interactions can be ignored, the calculated tensile stress distribution should be similar to that of thermal cracks when tensile (mode I) cracks open during temperature reduction. This approach could be taken further if physically reasonable crack distribution-permeability models are used to investigate fluid transport properties or the influence of crack distribution on seismic properties.

Piezoelectricity

The piezoelectric effect is the polarization of electric charge when differential stress is applied to a crystal. The phenomenon is characteristic of insulating crystals which lack a centre of symmetry, quartz and tourmaline being the best known examples. Polycrystalline aggregates of quartz may also be piezoelectric, depending on the ODFs of the right- and left-handed forms. The recent literature shows that whilst certain workers have found no measurable effect (Tuck *et al.* 1977), others report a strong effect (Bishop 1981, Nikitin & Parkhomenko 1982). The situation is all the more remarkable as both Tuck *et al.* (1977) and Bishop (1981) studied the same sample locality (Poughquag Quartzite from New York, originally described by Balk 1952). At least in part this controversy may be due to the difficulty in measuring the phenomenon, especially via static methods.

Laboratory measurements record two effects; one statistical, proportional to the number of grains in the specimen; one textural, due to the ODF. Thus, a specimen with a large grain size and relatively few grains may have an effect almost as important as in a single crystal in one sample and almost no effect in another sample from the same site. This would represent a statistical or sampling effect. The statistical effect is undoubtedly important in many of the Russian measurements as samples are almost exclusively taken from pegmatitic quartz veins (e.g. Parkhomenko 1971) which must be coarse grained. Undoubted textural piezoelectric effects have been reported by Bishop (1981) on three out of eight pure quartzites and 12 out of 100 gold-bearing quartz veins by Nikitin & Parkhomenko (1982). Ghomshei *et al.* (1988) report a strong **a** axes preferred orientation in a vein quartz sample with an important texturally related piezoelectric effect. Although it is theoretically possible to have a piezoelectric effect with equal proportions of right- and left-handed forms (Parkhomenko 1971), it seems more likely that a dominance of one enantiomorph is the cause (Bishop 1981). Why one enantiomorph is volumetrically dominant in a quartz vein is unknown. Tuck *et al.* (1977) speculated that it may be due to the presence of electrical currents during crystal growth, presumably during vein opening.

As previously mentioned, we have not determined the handedness of our individual measurements, all grains have been indexed as right-handed. Using this assumption, we have calculated the piezoelectric constants for Tongue quartzite. We have not assumed any particular stress tensor and present the results as contours in Coulombs Newton^{-1} (C N^{-1}). The complete triclinic sample symmetry piezoelectric tensor (18 constants) is determined in this manner, rather than the partial tensor (nine constants) experimentally determined by Bishop (1981) which correspond to orthorhombic sample symmetry. If we follow the IRE 1949 convention (see Bishop 1981) then the positive end of a right-handed quartz has a negative change in tensional stress. We see that the maximum effect ($\pm 0.59 \times 10^{-12}$ C N^{-1}) is 25.7% of the

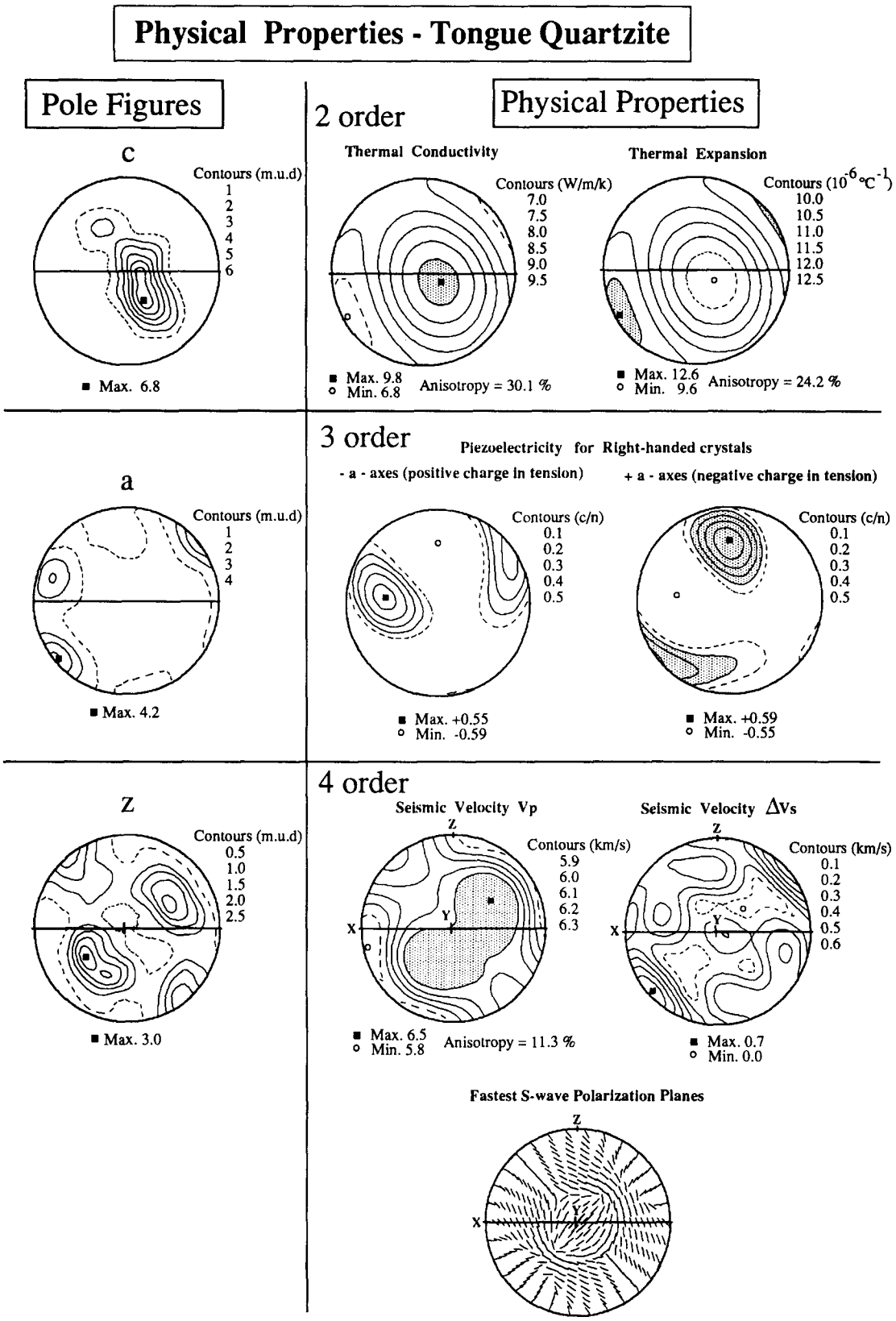

Fig. 10. Physical properties of Tongue quartzite. Second-order tensor properties thermal conductivity and thermal expansion. Third-order tensor property piezoelectricity, calculated assuming all the grains are right handed. Fourth-order seismic velocities V_p, ΔV_s and polarization plane of fastest S-wave. Pole figures of **c**, **a** and **z** are shown next to second-, third- and fourth-order properties to show the correlation between the texture and the property.

maximum single crystal value ($\pm 2.3 \times 10^{-12}$ C N^{-1}), which is of course much greater than the 0.1–0.01% typically encountered for statistical effects (Tuck *et al.* 1977, Bishop 1981) of quartzites. The maximum in the **a** pole figure (Fig. 10) corresponds to +**a** axes in the piezoelectric stereogram and the $+\mathbf{a}_2$ crystallographic axis in the IPF (Fig. 3). However, our assumption that all the grains are right-handed is unreasonable. In vein quartz a dominance of one hand has been reported (Frondel 1978). Perhaps a more reasonable assumption

is that there are one-third left and two-thirds right crystals as this could explain the strong asymmetry in the IPF (Fig. 3). In this case, the piezoelectric effect will be reduced to a maximum of 8.6% of the single crystal value, which is very close to the 7% value reported by Ghomshei *et al.* (1988) for a vein quartz.

Seismic properties

To calculate seismic properties from individual orientation measurements, we need to evaluate the elastic properties of the aggregate. For each orientation **g** the single crystal properties have to be rotated into the specimen co-ordinate frame using the orientation matrix g_{ij},

$$C_{ijkl}(\mathbf{g}) = g_{im} \cdot g_{jn} \cdot g_{ko} \cdot g_{lp} C_{mnop}(\mathbf{g}^o), \quad (12)$$

where $C_{ijkl}(\mathbf{g})$ is the elastic property in sample co-ordinates, **g** the measured orientation in sample co-ordinates and $C_{mnop}(\mathbf{g}^o)$ is the elastic property of quartz in crystal co-ordinates.

The elastic properties of the polycrystal may be calculated by integration over all possible orientations of the ODF. In the case of n individual orientation measurements from crystals of the same volume we can define the Voigt average of the quartz polycrystal as

$$\langle C_{ijkl} \rangle^{\text{Voigt}} = 1/n \, \Sigma \, C_{ijkl}(\mathbf{g}). \quad (13)$$

The final step is the calculation of the three seismic phase velocities by the solution of the Christoffel equation

$$\text{Det} | \langle C_{ijkl} \rangle^{\text{Voigt}} X_j X_l - \delta_{ik} \rho V^2 | = 0, \quad (14)$$

where $X_j X_l$ are the direction cosines of the wave propagation direction, δ_{ik} is the Kronecker delta, ρ the density of quartz and V is one of the three seismic phase velocities. Similar procedures can be used to calculate the Voigt, Reuss or Voigt–Reuss–Hill elastic averages and their corresponding seismic velocities. Measurements on the Twin Sisters Dunite by Crosson & Lin (1971) have shown that the seismic velocities calculated with the Voigt average give the closest agreement between velocities calculated using petrofabric data and laboratory measurements, and hence the Voigt average has been used for all the calculated velocities presented here.

P-wave velocities of Tongue quartzite (Fig. 10) show a strong anisotropy of 11% with a broad maximum of over 6.3 km s^{-1} near the Y structural axis. The topology of the maximum corresponds to that of the **z** pole figure, the maximum V_p being close to the **z** rhomb normal in a quartz single crystal. The minimum V_p is in the XZ structural plane with values below 5.9 km s^{-1}. The topology of the minimum is similar to that of the **a** and **m** pole figures as the minimum V_p is in the basal plane in single crystal quartz. The difference in shear wave velocity (ΔV_s), sometimes called 'shear wave splitting', shows a pronounced maximum of over 0.6 km s^{-1}. The topology of ΔV_s is very similar to the **a** pole figure. The polarization planes of the fastest S-wave has a very complex distribution which is not easily related to the texture. The V_p maximum can be correlated with a maximum density of **c** axes and the V_p minimum with the basal plane. Similar observations were made by Mainprice & Casey (1990) on a series of five quartzites and by Braun *et al.* (1991) on two quartzites where the textures were measured by X-ray goniometry. The SEM/ECP method has been applied to polyphase quartz-rich rocks by Barroul *et al.* (1992) for seismic studies where traditional texture measuring methods (e.g. U-stage or X-ray goniometry) are not applicable.

CONCLUSIONS

Recent advances in the electron optics and backscattered electron detectors of commercial SEMs, combined with computer-aided indexing allow the routine individual orientation determination of quartz grains using electron channelling patterns. In routine analysis it is not possible to determine the handedness of a quartz grain, all grains are indexed as right-handed. The ECP data can be used to study Dauphiné twinning, but not Brazil twinning. Textures resulting from centrosymmetric processes like dislocation glide will be completely characterized by the ECP data, whereas texture produced by non-centrosymmetric processes (e.g. grain boundary migration, Brazil twinning) will not be completely characterized. The ECP texture data (for example, from Tongue quartzite) provides a means of calculating all centrosymmetric physical properties (e.g. thermal conductivity, thermal expansion, seismic velocities), but not non-centrosymmetric properties such as piezoelectricity.

Individual orientation determination in quartz provides a new method for investigating local textures. Examples taken from Torridon 'quartzite' show that subgrains in individual grains have crystallographic axes which form dispersion trails, with an apparent rotation axis about the Y structural axis. Detailed analysis of the misorientation axes of the subgrains in specimen and crystallographic co-ordinates indicate a scattered distribution. We interpret the scatter as the influence of grain-scale strain incompatibilities as the dominant formation requirement for the subgrains, rather than the specimen scale kinematic flow. Unlike traditional texture analysis the information requires considerable interactive data processing as the link between micro structure and texture is important. Ideally the texture data should be mapped onto the micro structure, for example by plotting the orientation of each measurement point.

Acknowledgements—D. Mainprice thanks the C.N.R.S.-I.N.S.U. "DBT theme instabilities" No. 544 for financial support. D. Mainprice and G. E. Lloyd thank the British–French program ALLIANCE which provided the travelling funds that made this collaboration possible. D. Mainprice thanks Francis Wagner (Université de Metz) for the use of his individual orientation ODF program. The authors thank Professor H.-R. Wenk for his constructive editorial comments, Florian Heidelbach and an anonymous *JSG* reviewer for their reviews and Dr S. H. Kirby for the invitation to present this paper in the volume dedicated to Professor J. M. Christie. Our interest in quartz has been inspired by the pioneering work of John Christie on quartz

micro structures, petrofabrics and deformation mechanisms in the Moine thrust mylonites.

REFERENCES

Adams, B. L. & Field, D. P. 1992. Measurement and representation of grain-boundary texture. *Metall. Trans.* **23A**, 2501–2513.

Balk, R. 1952. Fabrics near thrust faults. *J. Geol.* **60**, 415–435.

Barruol, G., Mainprice, D., Kern, H., de Saint Blanquat, M. & Compte, P. 1992. 3D seismic study of a ductile shear zone from laboratory and petrofabric data (Saint Barthélémy Massif, Northern Pyrénées, France). *Terra Nova* **4**, 63–76.

Bishop, J. R. 1981. Piezoelectric effects in quartz-rich rocks. *Tectonophysics* **77**, 297–321.

Borradaile, G. J. & Hermes, J. J. 1980. Temporal changes in heat-flow distribution associated with metamorphism in the S.W. Scottish Highland and the Lepontine Alps. *J. Geol.* **88**, 87–95.

Braun, G., Siegesmund, S. & Dahms, M. 1991. The influence of quartz textures on the seismic anisotropy in lower crustal granulites. *J. Struct. Geol.* **13**, 955–966.

Buerger, M. J. 1930. Translation gliding in crystals. *Am. Mineral.* **15**, 45–64.

Bunge, H. J. 1982. *Texture Analysis in Materials Science*. Butterworths, London.

Bunge, H. J. & Esling, C. 1985. Symmetries in texture analysis. *Acta Cryst.* **A41**, 59–67.

Bunge, H. J. & Weiland, H. 1988. Orientation correlation in grain and phase boundaries. *Textures & Microstruct.* **7**, 231–263.

Christie, J. M. & Ardell, A. 1976. Deformation structures in minerals. In: *Electron Microscopy in Mineralogy* (edited by Wenk, H.-R.). Springer, Berlin, 374–403.

Connerney, J. E. P., Nekut, A. & Kuckes, A. F. 1980. Deep crustal electrical conductivity in Adirondacks. *J. geophys. Res.* **85**, 2603–2614.

Crosson, R. S. & Lin, J. W. 1971. Voigt and Reuss prediction of anisotropic elasticity of olivine. *J. geophys. Res.* **76**, 570–578.

Den Tex, E. 1975. Thermally mantled gneiss domes: the case for convective heat flow in more or less solid basement. In: *Progress in Geodynamics* (edited by Borradaile, G. J.). North-Holland, Amsterdam, 62–79.

Donnay, J. D. H. & Le Page, Y. 1978. The vicissitudes of the low-quartz setting or the pitfalls of enantiomorphism. *Acta Cryst.* **A34**, 584–594.

Faivre, G. & Le Goff, J.-J. 1979. Breakdown of Friedel's Law in the Kikuchi patterns of tellurium. *Acta Cryst.* **A35**, 604–610.

Field, D. P. & Adams, B. L. 1992. Heterogeneity of intergranular damage in copper crept in plane-strain tension. *Metall. Trans.* **23A**, 2515–2526.

Fitz Gerald, J. D., Etheridge, M. A. & Vernon, R. H. 1983. Dynamic recrystallization in a naturally deformed albite. *Textures & Microstruct.* **5**, 219–237.

Frondel, C. 1978. Characters of quartz fibres. *Am. Mineral.* **63**, 17–27.

Frondel, C. 1962. *Dana's System of Mineralogy, Volume III*. John Wiley, New York.

Gapais, D. & White, S. 1982. Ductile shear bands in a naturally deformed quartzite. *Textures & Microstruct.* **5**, 1–17.

Ghomshei, M. M., Narod, B. B., Templeton, T. L., Arrott, A. S. & Russell, R. D. 1988. Piezoelectric pole figures of a vein quartz sample. *Textures & Microstruct.* **7**, 303–316.

Goodman, P. & Johnston, A. W. S. 1977. Identification of enantiomorphously related space groups by electron diffraction—a second method. *Acta Cryst.* **A33**, 997–1001.

Goodman, P. & Secomb, T. W. 1977. Identification of enantiomorphously related space groups by electron diffraction. *Acta Cryst.* **A33**, 126–133.

Grimmer, H. 1980. A unique description of the relative orientation of neighbouring grains. *Acta Cryst.* **A36**, 382–389.

Grimmer, H. 1989. Coincidence orientations of grains in rhombohedral materials. *Acta Cryst.* **A45**, 505–523.

Grimmer, H. 1990. Special grain boundaries in rhombohedral materials. *J. Phys. Colloque C1* **51**, 155–160.

Heilman, P., Clark, W. A. T. & Rigney, D. A. 1982. Computerized method to determine crystal orientations from Kikuchi patterns. *Ultramicroscopy* **9**, 365–372.

Jessell, M. W. 1986. Grain boundary migration and fabric development in experimentally deformed octachloropropane. *J. Struct. Geol.* **8**, 527–542.

Kaufman, A. & Keller, G. 1981. *The Magnetotelluric Sounding Method*. Elsevier, New York.

Lister, G. S., Paterson, M. S. & Hobbs, B. E. 1978. The simulation of fabric development in plastic deformation and its application to quartzite: The model. *Tectonophysics* **45**, 107–158.

Lloyd, G. E. & Ferguson, C. C. 1986. A spherical electron channelling pattern map for the use in quartz petrofabric analysis. *J. Struct. Geol.* **8**, 517–526.

Lloyd, G. E., Ferguson, C. C. & Law, R. D. 1987. Discriminatory petrofabric analysis of quartz rocks using SEM electron channelling. *Tectonophysics* **135**, 243–249.

Lloyd, G. E., Law, R. D., Mainprice, D. & Wheeler, J. 1992. Microstructural and crystal fabric evolution during shear zone formation. *J. Struct. Geol.* **14**, 1079–1100.

Lloyd, G. E., Law, R. D. & Schmid, S. M. 1987. A spherical channelling patterns map for use in quartz petrofabric analysis: correction and verification. *J. Struct. Geol.* **9**, 251–253.

Lloyd, G. E., Schmidt, N. H., Mainprice, D. & Prior, D. J. 1991. Crystallographic textures. *Mineralog. Mag.* **55**, 331–345.

Mainprice, D., Bouchez, J.-L., Blumenfeld, P. & Tubià, J. M. 1986. Dominant *c* slip in naturally deformed quartz: Implications for dramatic plastic softening at high temperature. *Geology* **14**, 819–822.

Mainprice, D. & Casey, M. 1990. The calculated seismic properties of quartz mylonites with typical fabrics: relationship to kinematics and temperature. *Geophys. J. Int.* **103**, 599–608.

Mainprice, D., Humbert, M. & Wagner, F. 1990. Phase transformations and inherited LPOs—implications for seismic properties. *Tectonophysics* **180**, 213–228.

Marthinsen, K. & Høier, R. 1988. On the breakdown of Friedel's law in electron backscattering. *Acta Cryst.* **A44**, 700–707.

Matthies, S. 1979. On the reproducibility of the orientation distribution function of texture samples from pole figures (ghost phenomena). *Phys. Stat. Sol.* **B92**, 135–138.

Matthies, S. & Vinel, G. W. 1982. On the reproduction of the orientation distribution function of texturized samples from reduced pole figures using the conception of a conditional ghost correction. *Phys. Stat. Sol.* **B112**, 111–120.

McLaren, A. C. 1986. Some speculations in the nature of high-angle grain boundaries in quartz rocks. *Am. Geophys. Un. Geophys. Monogr.* **36**, 233–245.

McLaren, A. C. & Pitkethly, D. R. 1982. The twinning microstructure and growth of amethyst quartz. *Phys. Chem. Minerals* **8**, 128–135.

Nikitin, A. N. & Parkhomenko, E. I. 1982. Piezoelectric fabrics in quartz-bearing rocks and their symmetry properties. *Izvestiya Earth Phys.* **18**, 104–110.

Olesen, N. O. & Schmidt, N. H. 1990. The SEM/ECP technique applied on twinned quartz crystals. In: *Deformation Mechanisms, Rheology and Tectonics* (edited by Knipe, R. J. & Rutter, E. H.). *Spec. Publs geol. Soc. Lond.* **54**, 369–374.

Olhoeft, G. R. 1981. Electrical properties of granite with implications for the lower crust. *J. geophys. Res.* **86**, 931–936.

Parkhomenko, E. I. 1971. *Electrification Phenomena in Rocks*. Plenum, New York.

Pospiech, J., Sztwiertnia, K. & Haessner, F. 1986. The misorientation distribution function. *Textures & Microstruct.* **6**, 201–215.

Schaeben, H. 1988. Entropy optimization in texture goniometry I. Methodology. *Phys. Stat. Sol.* **B148**, 63–72.

Schmidt, N. H. & Olesen, N. O. 1989. Computer-aided determination of crystal-lattice orientation from electron-channeling patterns in the SEM. *Can. Mineral.* **27**, 15–22.

Shankland, T. J. 1981. Electrical conduction in the mantle materials. In: *Evolution of the Earth* (edited by O'Connell, R. J. & Fyfe, W. S.). American Geophysical Union, Washington, DC, 256–263.

Shankland, T. J. & Ander, M. E. 1983. Electrical conductivity, temperatures and fluids in the lower crust. *J. geophys. Res.* **88**, 9475–9484.

Smith, D. A. 1975. Microscopy of static and dynamic properties of interfaces. *J. Phys. Colloque C4* **10**, 1–15.

Trépied, L., Doukhan, J. C. & Paquet, J. 1980. Subgrain boundaries in quartz: Theoretical analysis and microscopic observations. *Phys. Chem. Minerals* **5**, 201–218.

Tuck, G. J. & Stacey, F. D. 1978. Dielectric anisotropy as a petrofabric indicator. *Tectonophysics* **50**, 1–11.

Tuck, G. J., Stacey, F. D. & Starkey, J. 1977. A search for the piezoelectric effect in quartz-bearing rocks. *Tectonophysics* **39**, T7–T12.

Tullis, J., Christie, J. M. & Griggs, D. T. 1973. Microstructures and preferred orientations of experimentally deformed quartzites. *Bull. geol. Soc. Am.* **84**, 297–314.

Urai, J. L., Means W. D. & Lister, G. S. 1986. Dynamic recrystallization of minerals. In: *Mineral and Rock Deformation, Laboratory Studies—The Paterson Volume* (edited by Hobbs, B. E. & Heard, H. C.). *Am. Geophys. Un. Geophys. Monogr.* **36**, 161–199.

Wagner, F., Wenk, H.-R., Esling, C. & Bunge, H. J. 1981. Importance of odd coefficients in texture calculation for trigonal-triclinic symmetries. *Phys. Stat. Sol.* **A67**, 269–285.

Wenk, E. 1970. Zur regionalmetamorphose und ultrametamorfose im Lepontin. *Fortschr. Miner.* **47**, 34–51.

Wenk, H.-R. 1985. *Preferred Orientation in Metals and Rocks: An Introduction to Modern Textural Analysis*. Academic Press, Orlando.

Wenk, H.-R., Bunge, H. J., Jansen, E. & Pannetier, J. 1986. Preferred orientation of plagioclase—neutron diffraction and U-stage data. *Tectonophysics* **126**, 271–284.

Wenk, H.-R., Bunge, H. J., Kallend, J. S., Lücke, K., Matthies, S., Pospiech, J. & Van Houtte, P. 1988. Orientation distributions: representation and determination. In: ICOTOM 8 *Textures of Materials* (edited by Kallend, J. S. & Gottstein, G.). The American Metallurgical Society, Warrendale, 17–30.

Wenk, H.-R. & Christie, J. M. 1991. Review Paper—Comments on the interpretation of deformation textures in rocks. *J. Struct. Geol.* **13**, 1091–1110.

Wenk, H.-R. & Wenk, E. 1969. Physical constants of Alpine rocks. *Schweiz. miner. petrogr. Mitt.* **49**, 343–357.

White, S. 1973. The dislocation structures responsible for optical effects in some naturally deformed quartzites. *J. Mater. Sci.* **9**, 490–499.